Supporting Information

Nanostructured Copper/Copper Oxides Hybrids: Combined Experimental and Theory Studies

Jie Li,[a] Nana Yu,[a] Haoran Geng[a,b]*

[a] School of Materials Science and Engineering, University of Jinan, West Nan Xinzhaung Road 336, Jinan 250022, PR China

[b] Shandong Provincial Key Laboratory of Preparation and Measurement of Building Materials, University of Jinan, West Nan Xinzhuang Road 336, Jinan 250022, P. R. China

Corresponding author: Haoran Geng

Email: 2013210163@mail.ujn.edu.cn

Tel / Fax: +86-0531-82765314

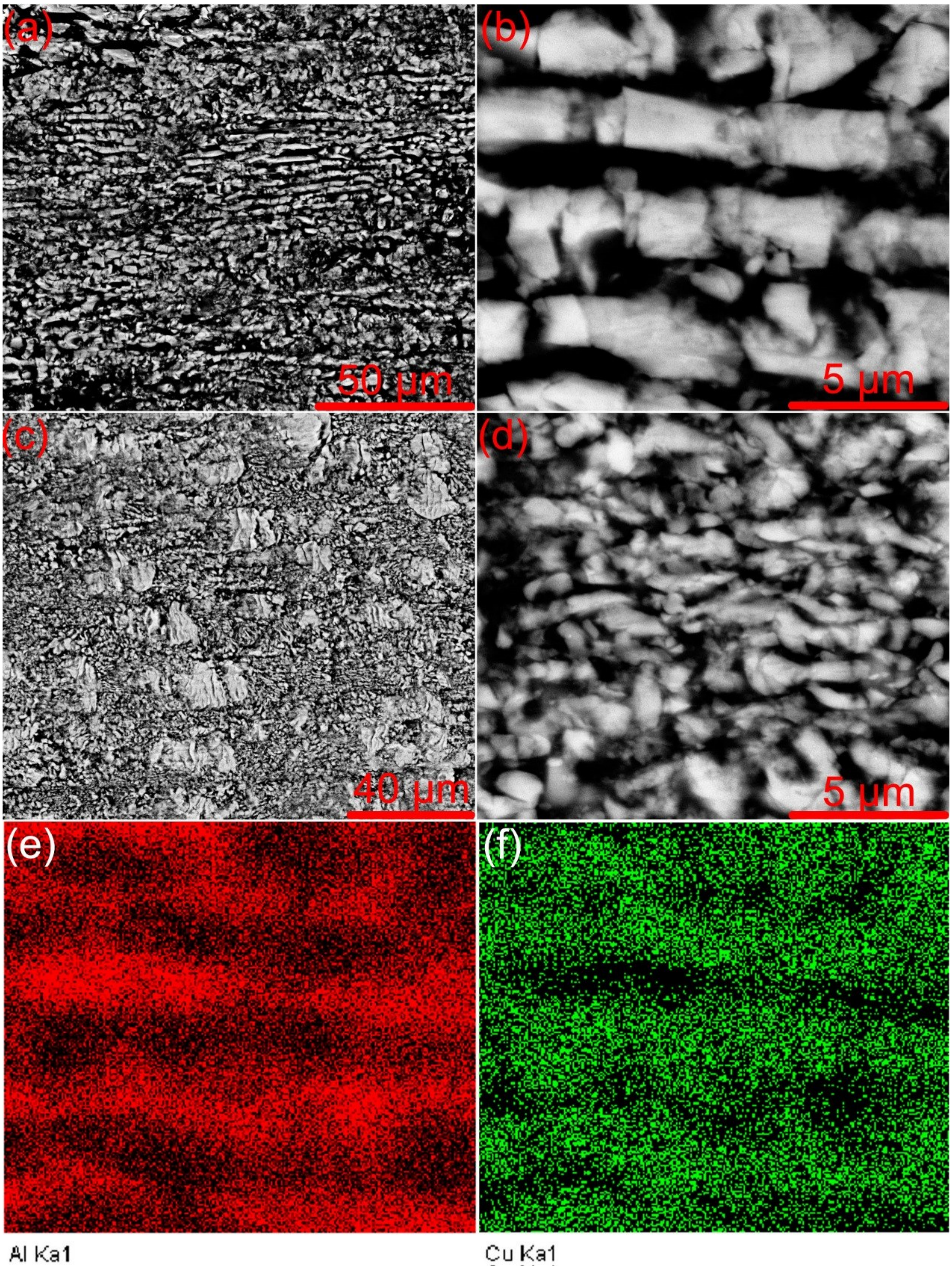

Figure S1. Back-scattering electron (BSE) images showing phases distribution of sintered $Al_{85}Cu_{15}$ (a,b) and cast $Al_{85}Cu_{15}$ (c,d). Elements mapping analysis of (e) and (f) respectively display Al and Cu distribution of the corresponding region in (b), showing that the white (black) region corresponds to Al_2Cu (Al) phase under the consideration of the XRD results in Figure 6, and the results are also true to cast $Al_{85}Cu_{15}$. (b) and (d) showing magnified images of the typical region in (a) and (c).

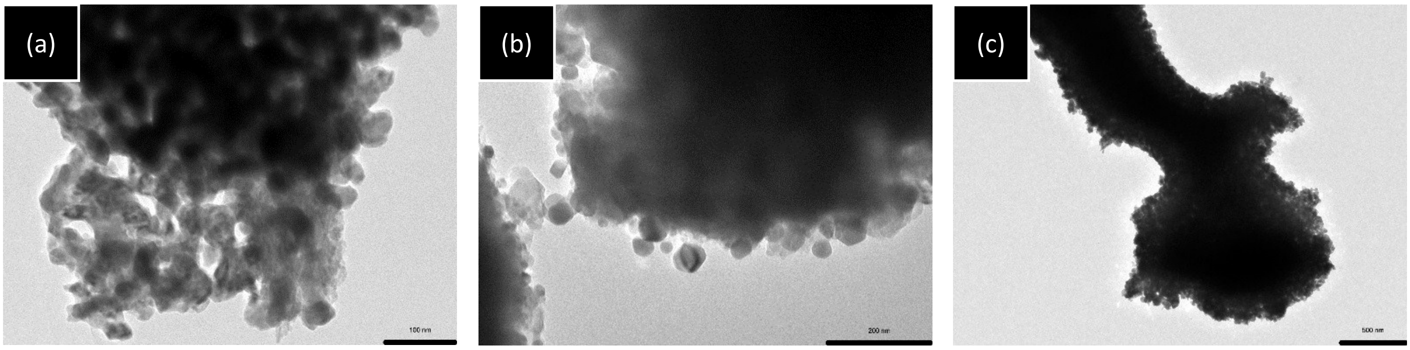

Figure S2. TEM micrographs showing the small magnification images of NPC (a), NPC/O (b), and heated-NPC (c).

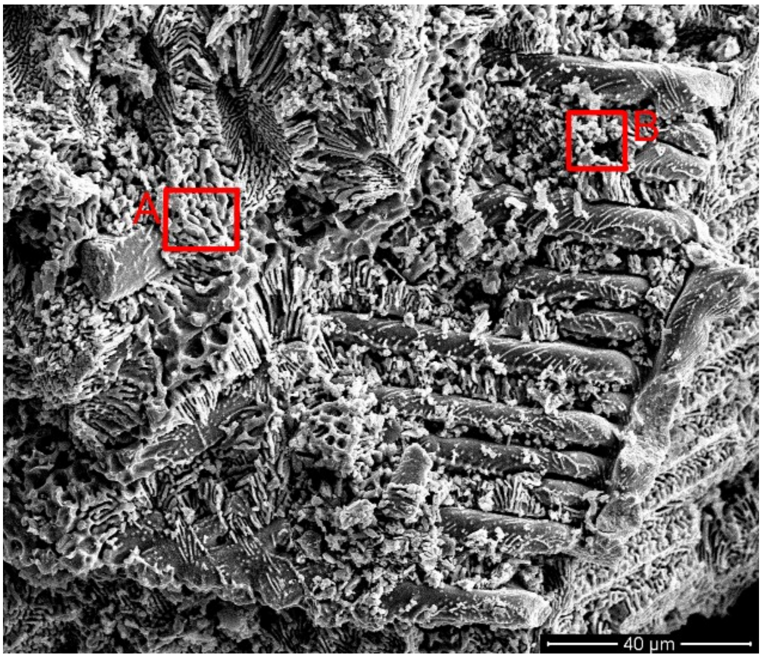

Figure S3. SEM micrographs showing the small magnification images of heated-NPC.

Table S1. Structure parameters of initial Al_2Cu and refined Al_2Cu in sintered $Al_{85}Cu_{15}$ precursor.

Parameters		Initial Al_2Cu	Refined Al_2Cu^a
Spacegroup		I4/mcm (140)	
a (Angstrom)		6.065	6.081
c (Angstrom)		4.873	4.866
Atom sites	Cu	(0, 0, 0.25)	(0, 0, 0.25)
	Al	(0.1581, 0.5581, 0)	(0.1217, 0.4970, 0.0641)

[a]: Rexp: 3.87%, Rwp: 9.60%, Rp: 6.09%, GOF: 2.48

Table S2. Snapshots of various Al-Cu systems at different time. Green balls represent Al and brown balls represent Cu.

Time (ps)	Structures		
	Al (1nm)-Cu (1nm)	Al (2nm)-Cu (2nm)	Al (4nm)-Cu (4nm)
0	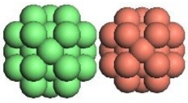	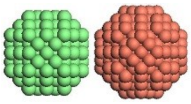	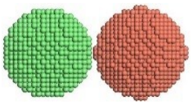
0 Energy minimizing	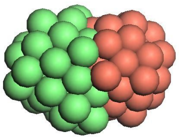	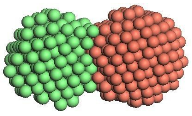	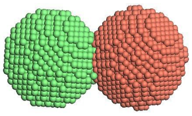
10	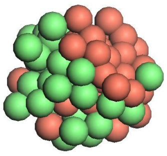	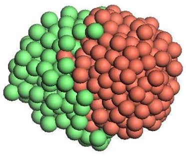	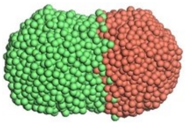
50	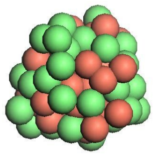	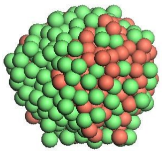	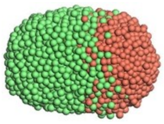
100	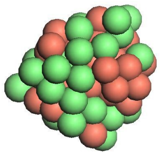	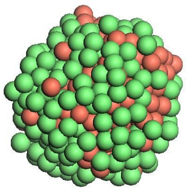	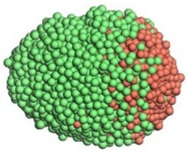
500	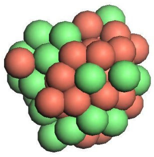	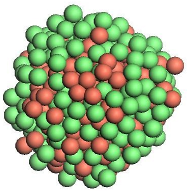	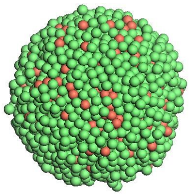
1000	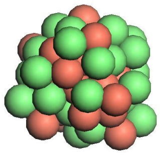	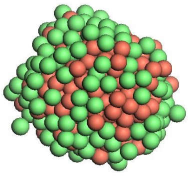	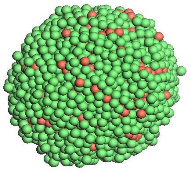
2000	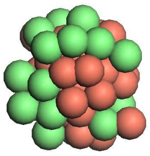	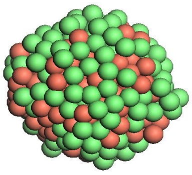	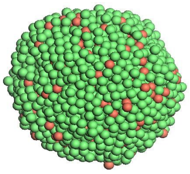
2000 (inner part)	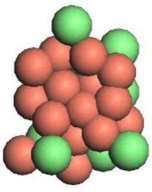	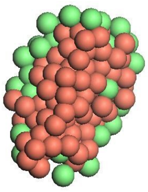	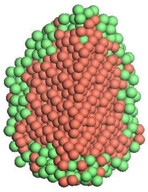

In this work, three models containing Al and Cu particles with varying diameters of 1nm, 2 and 4nm were also studied (Table S2). All systems were energy minimized (0 ps) followed by MD equilibrations of 2000 ps. Snapshots of these systems at various time are presented in Table S2. Initially, after energy minimizing the particle suffers distortions to different extent in order to release some stress and simultaneously two particles are attracted by each other. When MD simulations start Al and Cu atoms diffuse to each other and their snapshots vary with the system sizes. For smallest system, Al (1nm)-Cu (1nm), Al and Cu atoms diffuse dramatically and the system turns a round particle at 10 ps. When it is 50 ps, Al and Cu atoms appear to uniformly distribute in particle and this situation remains in the following 1950 ps though atoms randomly diffuse. When the system is enlarged to Al (2nm)-Cu (2nm), Al and Cu atoms diffuse to each other and the system becomes an ellipsoid at 10 ps. When MD simulation continues to 100 ps the system gradually turns a round particle and Cu cluster is nearly fully covered by Al atoms, indicating the faster diffusion of Al atoms than Cu atoms. In the following simulation process Al and Cu atoms keep diffusing but the system does not change much as shown in Table S2, especially from 1000 ps and 2000 ps. For a bigger system, Al (4nm)-Cu (4nm), the atoms diffusions and cluster evolution are similar to those of Al (2nm)-Cu (2nm) within 2000 ps. As shown in Table S2, the inner structures of all Al-Cu systems are also studied. It is evident that all Al-Cu systems are composed of Cu core and Al shell, with only a few Al atoms permeating into Cu core. In other words, it is far away from diffusion equilibrium within 2000 ps even though for a smallest system of Al (1nm)-Cu (1nm). It is clear, however, Al (4nm)-Cu (2nm) system reaches equilibrium at 1000 ps (see Table 1).

It should be noted that Al/Cu ratios of Al (1nm)-Cu (1nm), Al (2nm)-Cu (2nm) and Al (4nm)-Cu (4nm) systems are respectively 1:1, 0.67:1 and 0.68:1 which are very different from that (5.67:1) of actually $Al_{85}Cu_{15}$ alloys. And the phenomena mentioned above can be explained by chemical potential which plays an important role in atom diffusion[1]. The chemical potentials of Al and Cu in Al-Cu systems can be calculated as following[2]:

$$\mu_i = G_i + \mathrm{RT}\ln x_i$$

where i is Al or Cu in Al-Cu systems, G_i is the standard chemical potential of pure element, and G_{Al} and G_{Cu} are 6.61×10^3 J/mol and 8.37×10^3 J/mol, respectively [3, 4]. R is ideal gas constant (8.314 J/(mol*K)), T is temperature (1000K) and x_i is the percentage of component i. The calculated chemical potentials of Al and Cu in each Al-Cu systems are listed in Table S3. Evidently, the chemical potentials of Al in Al (1nm)-Cu (1nm), Al (2nm)-Cu (2nm) and Al (4nm)-Cu (4nm) are much smaller than those of Cu in these systems. For Al(4nm)-Cu (2nm) in which Al/Cu ratio is close to that (5.67:1) of actual $Al_{85}Cu_{15}$ alloy, chemical potential of Al is higher than that of Cu. That is why Al(4nm)-Cu (2nm) system reach equilibrium within 1000 ps while Al(1nm)-Cu (1nm) system is composed of Cu(core)@Al(shell) structure even though MD time is 2000 ps.

Table S3. Al/Cu ratios and chemical potentials of Al and Cu in each Al-Cu systems.

Systems	Al/Cu ratio	Chemical potentials（J/mol）	
		Al	Cu
Al (1nm)- Cu (1nm)	1:1	847.2	2607.2
Al (2nm)- Cu (2nm)	0.67:1	-983.2	4106.4
Al (4nm)- Cu (4nm)	0.68:1	-909.6	4056.7
Al (4nm)- Cu (2nm)	5.36:1	5187.8	-7011.1

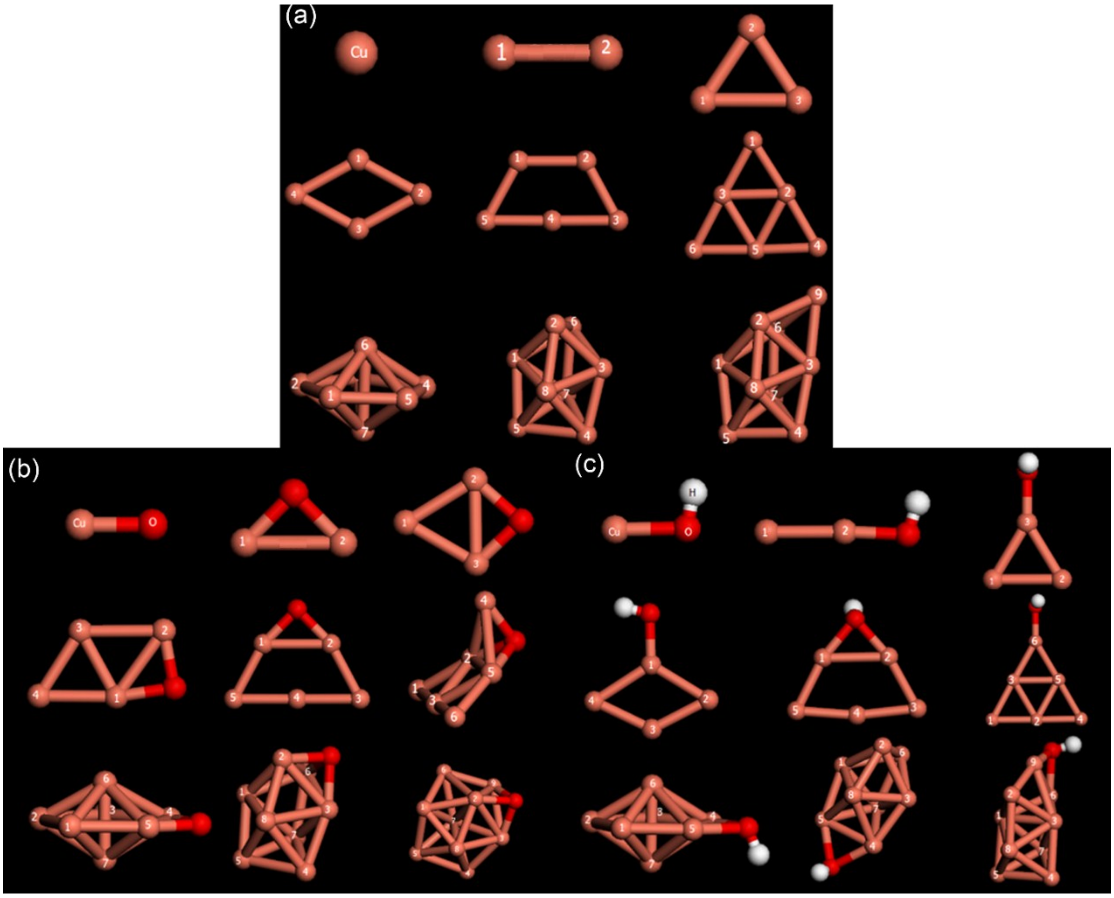

Figure S4. Optimized ground-state geometries of Cu_n (a) Cu_n-O (b) and Cu_n-OH^- (c) ($1 \le n \le 9$). Brown balls: Cu, white balls: hydrogen atom (H) and red balls: oxygen atom (O).

The optimized geographies of neutral copper clusters (Cu_n) and adsorbed systems (Cu_n-O and Cu_n-OH^-) having the lowest energy among their isomers are displayed in Figure S4. The ground-state geometries of the neutral Cu_n (n=1-6) are planar, they are similar to the corresponding gold clusters as well as other reports about copper clusters[5, 6]. The geometry starts to be three-dimensional structures when n reaches 6. When the atom numbers increase to 7, copper cluster is in form of pentagon bipyramid with the two capping atoms forming a bond. When the cluster grows, it becomes more closely packed. A counterpart copper of a vertex of pentagon makes Cu_8 looks like a cage. In Cu_9, the new addition copper atom forms a cap. When the copper clusters combine with O or OH^-, copper clusters' structures does not change too much except for Cu_6-O, in which one copper atoms is folded. In addition, when $n \le 5$ oxygen atoms are bridged to Cu_n except for Cu_1-O in which O is top-type adsorbed as seen in Figure S4b. It is also true to Cu_7, oxygen atom is adsorbed on bridge type site and it stays on the pentagon plane. When n is 6, 8 and 9 the oxygen atom is adsorbed on a three-fold hollow type site. When it refers to OH^-, it is clear that OH^- are adsorbed either on top type sites (n=1, 2, 3, 4, 6) or on the bridge type sites (n=5, 7, 8, 9), as shown in Figure S4c.

Fukui indices have been proved to be an effective parameter to analyze the local reactivity, and it is an indication of the reactive centers in the molecular [7, 8]. In finite difference approximation[9], the condensed Fukui functions at atom k can be calculated as follows:

$$\text{(nucleophilic attack)} \qquad f^+ = q_k(\mathrm{N}) - q_k(\mathrm{N}+1) \qquad (1)$$

$$\text{(electrophilic attack)} \qquad f^- = q_k(\mathrm{N}-1) - q_k(\mathrm{N}) \qquad (2)$$

Where q_k is the gross charge of atom k in the cluster and N is the number of electrons. And in the clusters, the regions of higher f^+ values are assigned as active regions for the reaction with oxygen.

Table S4 gives the condensed Fukui indices (f^+) of Cu_n clusters and they are evaluated from Mulliken population analysis of atoms in Cu_n. It should be pointed out that oxygen atom is mainly adsorbed on the copper atoms (marked by numbers in Figure S4) which have the largest or relatively larger value of f^+(the corresponding values are italicized and bolded in the table S4). Even though the exceptions of Cu_7-O and Cu_7-OH^- systems in which the involved copper atoms have relatively smaller f^+ values, it could be arrived that Fukui indices is effective and accurate to be used to predict active sites on which oxygen atoms are adsorbed. After adsorption, the f^+ values of involved copper atoms decrease (Table S5), indicating the electron transfer from cluster to oxygen[10, 11].

Table S4. Calculated condensed Fukui indices of Cu_n.

	f_1^+	f_2^+	f_3^+	f_4^+	f_5^+	f_6^+	f_7^+	f_8^+	f_9^+
Cu_1	***1.0***								
Cu_2	***0.5***	***0.5***							
Cu_3	0.259	***0.461***	***0.28***						
Cu_4	***0.341***	***0.159***	0.341	0.159					
Cu_5	***0.222***	***0.227***	0.209	0.131	0.211				
Cu_6	0.261	0.072	0.07	***0.267***	0.071	***0.259***			
Cu_7	0.098	0.1	0.095	0.098	0.105	***0.252***	***0.252***		
Cu_8	0.069	***0.195***	0.063	***0.185***	***0.174***	***0.176***	0.07	0.067	
Cu_9	0.071	0.065	0.058	0.111	0.249	0.069	0.063	0.063	***0.252***

Table S5. Calculated condensed Fukui indices of Cu_n-O.

	f_1^+	f_2^+	f_3^+	f_4^+	f_5^+	f_6^+	f_7^+	f_8^+	f_9^+	f_O^+
Cu_1-O	0.524									0.476
Cu_2-O	0.434	0.433								0.134
Cu_3-O	0.415	0.219	0.218							0.148
Cu_4-O	0.142	0.283	0.195	0.257						0.123
Cu_5-O	0.142	0.144	0.218	0.135	0.218					0.143
Cu_6-O	0.152	0.093	0.125	0.344	0.092	0.152				0.042
Cu_7-O	0.116	0.28	0.127	0.135	0.134	0.056	0.068			0.084
Cu_8-O	0.067	0.125	0.109	0.118	0.231	0.12	0.087	0.092		0.05
Cu_9-O	0.092	0.103	0.106	0.119	0.211	0.104	0.04	0.091	0.075	0.06

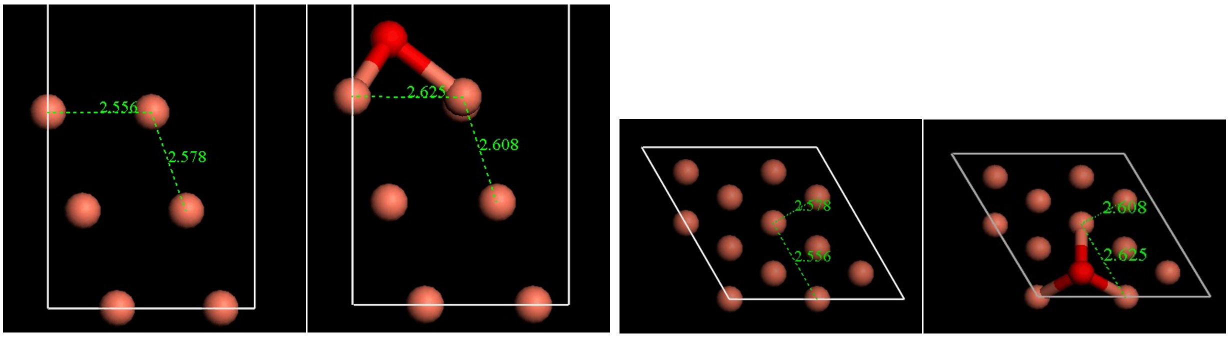

Figure S5. Optimized geometries of side views and top view of Cu(111) and Cu(111)-O, respectively (from left to right). Red balls: oxygen atom and brown atoms: Cu. Calculations were performed with the bottom atoms fixed and top topmost atoms unfixed. Clearly, after simulating distances between top atoms and second layer atoms are enlarged and it is also applied to the distance among top atoms.

References

1. J. Jäckle and H. L. Frisch, *Journal of Polymer Science: Polymer Physics Edition*, 1985, **23**, 675-682.
2. M. Piro, T. M. Besmann, S. Simunovic, B. Lewis and W. Thompson, *J. Nucl. Mater.*, 2011, **414**, 399-407.
3. E. Wiberg, *Die chemische Affinität: eine erste Einführung in die Lehre von der Triebkraft chemischer Reaktionen*, Walter de Gruyter, 1972.
4. E.-U. N. b. o. standards, H. Prophet and D. R. Stull, *JANAF thermochemical tables: DR Stull and H. Prophet project directors*, US Government Printing Office, 1971.
5. S. Baishya and R. C. Deka, *Int. J. Quantum Chem.*, 2014, **114**, 1559-1566.
6. G. H. Guvelioglu, P. P. Ma, X. Y. He, R. C. Forrey and H. S. Cheng, *Phys. Rev. Lett.*, 2005, **94**, 026103.
7. P. Fuentealba, E. Florez and W. Tiznado, *J. Chem. Theory Comput.*, 2010, **6**, 1470-1478.
8. R. K. Roy, K. Hirao, S. Krishnamurty and S. Pal, *The Journal of Chemical Physics*, 2001, **115**, 2901-2907.
9. W. Yang and R. G. Parr, *Proceedings of the National Academy of Sciences*, 1985, **82**, 6723-6726.
10. L. PADILLA-CAMPOS, *J. Chil. Chem. Soc.*, 2005, **50**, 745-752.
11. X. Guo, B. Teng, J. Yuan, Y. Zhao, Y. Zhao and S. Liu, *Acta Phys. -Chim. Sin.*, 2011, **27**, 1068-1074.